2-Thiophenyl–Isoquinoline Ir(III) Complex: A Promising Tool in Antipseudomonal Photodynamic Therapy under Red Irradiation

Julien Renault, Julie Couchot, Aline L Faucon, Jean-luc Renaud, Gaëtan L A Mislin, Patrick Plésiat, Sylvain Gaillard

EurJIC
European Journal of Inorganic Chemistry

Research Article
doi.org/10.1002/ejic.202300767

Chemistry Europe
European Chemical Societies Publishing

www.eurjic.org

2-Thiophenyl–Isoquinoline Ir(III) Complex: A Promising Tool in Antipseudomonal Photodynamic Therapy under Red Irradiation

Julien Renault[+],[a] Julie Couchot[+],[b] Aline L. Faucon,[c, d] Jean-Luc Renaud,[a, e] Gaëtan L. A. Mislin,*[c, d] Patrick Plésiat,*[b] and Sylvain Gaillard*[a]

Innovative therapeutic strategies are more than ever needed to counter the rise of antibiotic–resistant bacterial pathogens worldwide. The use of light, and especially photodynamic therapy (PDT) appears as a promising alternative or complement to antibiotic treatments, fostered by the development of new photosensitizers. In this study, eight Ir(III) complexes were synthesized and evaluated for their photoactivation properties and capacity to generate radical species under blue (452 nm), green (525 nm), and red (631 nm) LED light, respectively. Their antibacterial properties were assessed on *Pseudomonas aeruginosa*, *Acinetobacter baumannii*, *Escherichia coli*, and *Staphylococcus aureus* with most of these complexes exhibiting potentially useful activities upon light irradiation, at concentrations below 10 mg/L. A complex of Ir(III) cyclometallated to thiophenyl–isoquinoline (tiq) and bearing 2,2′-bipyridine (bipy) as ancillary ligand was further investigated. This latter showed a concentration- and light intensity–dependent bactericidal activity on *P. aeruginosa* when irradiated under blue to red lights, proving that such complexes would be suitable candidates for PDT. Importantly, this lead complex remained active against antibiotic resistant clinical strains and was unaffected by active efflux systems. These data open interesting perspectives for the development of new treatments to tackle antibiotic resistant Gram–negative bacteria.

Introduction

Bacterial resistance to the current antibiotic arsenal has become a major sanitary issue in many countries, and new therapeutic strategies to combat difficult–to–treat infections are eagerly awaited.[1,2] The antibiotic molecules approved so far in human medicine are mainly based on elements from the three first periods of the Mendeleev's table (namely, hydrogen, carbon, nitrogen, oxygen, sulphur, and phosphorus). Other elements of the periodic table have been poorly investigated and can *de facto* be considered as a potential source of innovation to combat multidrug resistant pathogens. Due to their intrinsic toxicity towards human and animal cells, these latter have been reserved thus far to the treatment of heavy pathologies such as cancers and autoimmune diseases.[3–6] However because of the increasing administration of last resort antibiotics (e.g., polymyxins) known to be notoriously toxic,[7] the benefit/risk balance offered by metal containing antibiotics worth being reconsidered.[6,8–10]

Organometallic derivatives can possess an intrinsic antibacterial activity. More interestingly, depending on the nature of the metal and organic moieties, some complexes can be activated with light to generate reactive oxygen species (ROS), and could therefore be employed as photosensitizers (PS) in antibacterial photodynamic therapy (PDT).[11–18] In this booming field, ruthenium complexes have been particularly investigated for their light–promoted antibacterial activity.[11–14] Other metallic complexes were evaluated more scarcely. As potential antibacterials, iridium complexes offer interesting properties,[15–18] such as a good photostability and a compatible redox potential at excited state for ROS generation during the irradiation time.[19,20] In addition, the hexacoordination mode can limit its degradation upon nucleophilic attacks onto the metal centre in the biological media.[21] Previously, we reported that Ir(III) complexes bis–cyclometallated with 2-phenylisoquinoline (piq) and bearing 2,2′-dipyridylamine derivatives as ancillary ligand, exhibit an intrinsic activity on both free–living (i.e., planktonic) and sessile (i.e., forming biofilm) cells of the opportunistic pathogen *Pseudomonas aeruginosa*. Furthermore, this antibacterial activity was significantly increased under blue LED light.[18] Recent reports confirm the potential of iridium complexes in antibacterial PDT.[14–18] In PDT, the wavelength of

[a] *Dr. J. Renault,[+] Prof. J.-L. Renaud, Dr. S. Gaillard*
Normandie University, LCMT, ENSICAEN, UNICAEN, CNRS
6 Bd du Maréchal Juin, 14050 Caen, France.
E-mail: sylvain.gaillard@ensicaen.fr

[b] *J. Couchot,[+] Prof. P. Plésiat*
Université de Franche-Comté, UMR6249 CNRS Chrono-environnement
19 rue Ambroise Paré, 25000, Besançon, France
E-mail: patrick.plesiat@univ-fcomte.fr

[c] *Dr. A. L. Faucon, Dr. G. L. A. Mislin*
CNRS, UMR7242 Biotechnologie et Signalisation Cellulaire 300 Boulevard Sébastien Brant, F-67412 Illkirch, Strasbourg, France

[d] *Dr. A. L. Faucon, Dr. G. L. A. Mislin*
Université de Strasbourg, Institut de Recherche de l'Ecole de Biotechnologie de Strasbourg (IREBS)
300 Boulevard Sébastien Brant, F-67412 Illkirch, Strasbourg, France

[e] *Prof. J.-L. Renaud*
Sorbonne Université, CNRS, Institut Parisien de Chimie Moléculaire, UMR 8232, 75005 Paris, France

[+] *Authors have contibuted equally*

Supporting information for this article is available on the WWW under https://doi.org/10.1002/ejic.202300767

Research Article
doi.org/10.1002/ejic.202300767

emitting light source is crucial, not only to optimize the antibacterial efficacy of PS but also to limit side–effects on host tissues.[22] Indeed, while blue light is antibacterial by itself by activation of endogenous PS including porphyrins and flavines, it can be deleterious to irradiated tissues as these PS are also present in host cells.[23] Red–shifting of the excitation wavelength to green or red region is expected to improve light penetration up to the infection site while limiting damages to the surrounding cells.[24,25] In this context, the development of red–absorbing PS is of great interest in PDT strategies. The literature is particularly well–documented about the photophysical/structural relationships for iridium complexes where the most important electronic transition is the ^{3}MLCT to generate strongly bactericidal radical oxygen species such as superoxide anion $O_2^{\cdot-}$.[26] A brief survey of the literature shows that the ^{3}MLCT is mainly driven by the electronic properties of the cyclometallated ligand. To generate red-shift of the absorption wavelength, it is commonly accepted that introduction of heavier atoms or extension of the π-system can lead to such red–shift.

The present study describes the synthesis, the photophysical and electrochemical properties as well as photogeneration of ROS under blue (452 nm), green (525 nm), or red (631 nm) LED light irradiation, of a set of eight Ir(III) complexes. Their antibacterial properties were investigated *in vitro* on four major human pathogens. The most promising complex demonstrated a concentration- and light intensity–dependent bactericidal activity on the nosocomial bacterium *P. aeruginosa*. Unaffected by antibiotic resistance mechanisms including efflux pumps, this complex remained uniformly active on multidrug resistant clinical strains of *P. aeruginosa*.

Results and Discussion

Synthesis

For our study on the impact of the excitation wavelength on antibacterial activity, we selected cyclometallating ligands such as *N*-phenylpyrazole (ppz, **L1**), 2-phenylisoquinoline (piq, **L2**) and coumarin C6 (C6C, **L3**) expecting to furnish iridium (III) complexes emitting in the UV, blue and green regions, respectively (Figure 1). Finally, exploring the literature and following some well–known strategies to red–shift absorption wavelength for iridium complexes, the 2-thiophenyl-isoquinoline (tiq, **L4**) was envisaged to design new red–absorbing PS.[27] For comparison with our previous results, 2,2′-dipyridylamine (dpa, **L5**) was at first selected as ancillary ligand, and also the more commonly encountered 2,2′-bipyridine (bipy, **L6**) in order to evaluate the potential electronic behaviour of the electronic properties of the ancillary ligand. Indeed, the presence of heteroatom between the two pyridine rings can potentially have strong impact on the photophysical properties of transition metal complexes.

For the synthesis of the cationic iridium (III) complexes, Nonoyama's protocol was selected as standard procedure.[28,29] Briefly, formation of μ–chloro–bridged iridium dimers **1** to **4**

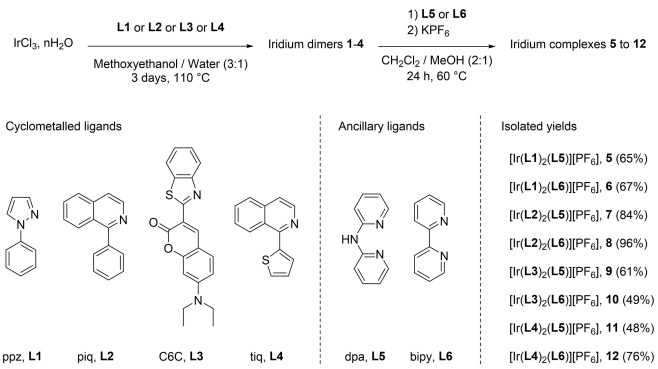

Figure 1. Selected iridium complexes and their synthesis.

were achieved using ligands **L1** to **L4** and further engaged with the ancillary ligands **L1** or **L2** (Figure 1) furnishing our library of eight cationic iridium (III) complexes **5** to **12** with isolated yields ranging from 48 to 96% for the second step.[30–32] All complexes were fully characterized by usual spectroscopy analysis (see ESI).

Photophysical and Electrochemical Characterization

The UV-Visible spectra of the iridium complexes **5** to **12** were recorded in dichloromethane at 298 K (Figure 2, Table 1).

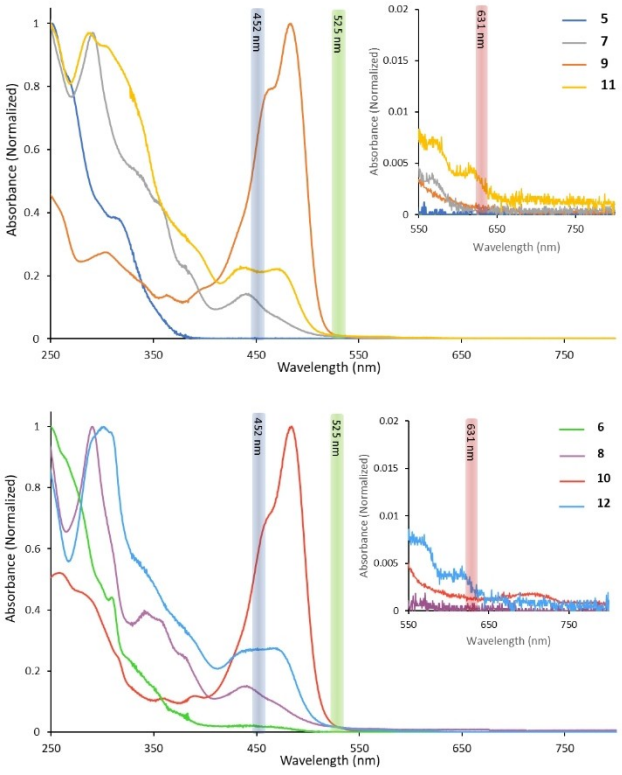

Figure 2. UV-visible spectra of **5** to **12** in dichloromethane solution (10^{-5} M). Inset is a zoom of the red region of the UV-visible spectra. Wavelengths of the maximum emission of the LEDs used in our set up for anti–bacterial assays are also represented with blue, green and red bars.

Table 1. Photophysical characterization of **5**–**12** in solution.

Complex	Absorption[a]	Emission[b]		
		λem (nm)	Φ	τ (ns)
[Ir(**L1**)$_2$**L5**][PF$_6$] **5**	252(4.62), 269(4.53), 317(4.21), 359(3.43)	334	<0.01	0.7 and 3.2
[Ir(**L1**)$_2$**L6**][PF$_6$] **6**	267(33.9), 309(17.1), 352(5.5), 442(0.8)	575	0.16	231
[Ir(**L2**)$_2$**L5**][PF$_6$] **7**	291(49.1), 334(25.3), 359(20.2), 386(10.2), 429(6.0)	639	0.09	680
[Ir(**L2**)$_2$**L6**][PF$_6$] **8**	292(54.2), 309(33.5), 340(20.9), 361(18.4), 438(8.1)	634	0.09	596
[Ir(**L3**)$_2$**L5**][PF$_6$] **9**	254(39.4), 305(24.4), 397(13.9), 463(69.9), 484(88.4)	592	0.04	3.7 and 2120
[Ir(**L3**)$_2$**L6**][PF$_6$] **10**	265(56.6), 284(50.9), 391(12.5), 461(74.1), 485(105.3)	593	0.02	4.2 and 1590
[Ir(**L4**)$_2$**L5**][PF$_6$] **11**	290(39.6), 350(20.5), 433(8.9)	633	0.05	451
[Ir(**L4**)$_2$**L6**][PF$_6$] **12**	298(35.0), 343(19.3), 385(11.5), 438(9.5)	630	0.04	503

[a] Absorption maxima and molar absorption coefficient in parenthesis in dichloromethane solution. [b] In deaerated dichloromethane solution c = 1.10^{-5} M using an excitation wavelength of 310 nm (**5** et **6**) or 450 nm (**7**–**12**).

Iridium complexes **5** and **6**, bearing ppz (**L1**), exhibited absorption bands mainly localized in the UV region at 250 to 360 nm range, assigned to a strong contribution of ligand centered transitions (LC). Of note, the slightly yellow coloured complex **6** showed a weak maximum absorption (λ_{abs}) at 442 nm (molar extinction (ε) of 800 $M^{-1}.cm^{-1}$) that could be assigned to the spin allowed metal to ligand charge transfer (^{1}MLCT) and/or the spin forbidden metal to ligand charge transfer (^{3}MLCT) band as proposed in the literature for some close congeners.[33,34] Then, iridium complexes **7** and **8** cyclometallated to piq (**L2**) showed absorption in the blue region with λ_{abs} centered at 429 and 438 nm (ε of 6 000 $M^{-1}.cm^{-1}$ for **7** and 5 800 $M^{-1}.cm^{-1}$ for **8**). The latter absorption bands of complexes **7** and **8** can be assigned to the spin allowed singlet charge–transfer (^{1}CT).[35] Of note, tails of the absorption bands of **7** and **8** were noticed to extend until wavelengths corresponding to the green region, i.e. up to 525 nm. This extension of the last absorption band has been assigned in the literature to triplet charge transfer (^{3}CT) and more precisely to a ligand–to–ligand charge transfer (LLCT) from **L2** to ancillary ligand **L5** or **L6** with an overlap of a ^{3}MLCT.[35] Then, **9** and **10** bearing ligand Coumarin 6 (C6 C, i.e. **L3**) showed absorption from the blue to green region with strong maxima at 484 and 485 nm (ε of 88 400 $M^{-1}.cm^{-1}$ and 105 300 $M^{-1}.cm^{-1}$, respectively). This large and intense absorption exhibited by **9** was assigned to the ^{1}MLCT transition,[36] and by analogy for **10**, as a same absorption profile was observed in both UV-visible spectra. Finally, **11** and **12** bearing ligand tiq (**L4**) possessed absorption ability in the blue–green region with maxima at 433 nm for **11** (ε of 8 900 $M^{-1}.cm^{-1}$), and 438 nm for **12** (ε of 8900 $M^{-1}.cm^{-1}$). The maximum absorption band in the blue region for **11** and **12** could be assigned to ^{1}LC and ^{1}MLCT. Finally, UV-visible spectra of **11** and **12** also exhibited a weak absorption from the tail of the spectra going up to wavelengths corresponding to the red region that could be assigned to a ^{3}MLCT by analogy of the homoleptic tris **L4** iridium (III) complex reported in the literature.[37] Figure 2 represents the UV-visible spectra of **5** to **12** split in function of the ancillary ligand **L5** or **L6**, and the maximum emission wavelengths of the LEDs used for the set up during the photoactivation of the PS in the antibacterial assays (Table 1 and see also Figure S21 to S28 in ESI). Anticipating the determination of the photoredox properties of our complexes, phosphorescent emissions were then recorded for **5** to **12** to further estimate the redox potentials at the excited state. **7** to **12** displayed orange to red emission with λ_{em} found between 592 to 633 nm. A lower emission wavelength (334 and 575 nm) was observed for **5** and **6** bearing **L1**. The photoluminescent quantum yields (PLQY) of these complexes recorded in deaerated dichloromethane at 298 K were found to range from 0.02 to 0.16 except for complex **5** that exhibited very weak emission. In details, ancillary ligand **L5** or **L6** did not appear to drastically modify quantum yields and emission wavelengths when associated with a same cyclometallating ligand, **L2** to **L4**. Only **5** and **6** showed very different emission properties, and only the ancillary ligand **L5** led to a very weak emissive complex with PLQY below 0.01. Lifetimes of the excited state of PS **5** to **12** were also measured in deaerated dichloromethane at 298 K as it can be a key parameter in the electron transfer process onto O_2 for the generation of ROS. **7**, **8**, **11** and **12** exhibited mono–exponential and close lifetimes of hundreds nanosecond range (451 to 680 ns) which is typical for iridium (III) PS.[35] **9** and **10** exhibited a bi–exponential lifetime with a short component (3.7 and 4.2 ns, respectively) likely coming from a fluorescence contribution of the ligands, and a longer component of the micro second order (2.12 and 1.59 μs, respectively) potentially due to a phosphorescence contribution. It can be noted that the long component lifetime in the decays of **9** and **10** are 3 or 4 times longer than the phosphorescence of **7**, **8**, **11** and **12**. Then, **6** exhibited a mono exponential decay like **7**, **8**, **11** and **12** but with a shorter lifetime compared to **7**, **8**, **11** and **12** (231 ns vs. 451 to 680 ns). Once again, complex **5** presented a very different behaviour as its lifetime exhibited a bi–exponential decay with two very short components of nanosecond order (0.7 and 3.2 ns).

Then, voltammograms of **5** to **12** were recorded in deaerated acetonitrile to determine redox potential at the ground state (Figures S30 to S37 in ESI). Reversible oxidation

Research Article
doi.org/10.1002/ejic.202300767

waves were observed at values between 1.05 to 1.29 V vs Saturated Calomel Electrode (SCE) for **5** to **12** corresponding to the metal centred E_{ox} process (Table 2).[38,39]

Finally, the redox potential at the excited state E^*_{ox} of **5** to **12** were approximated using their emission wavelength for the calculation of the photoactivation energy E_{00}.[40,41] The redox potential E^*_{ox} of **5** to **12** were then between −0.78 to −2.42 V. If compared to the redox potential of the couple $O_2/O_2^{\cdot-}$(−0.75 V vs SCE), the values of the redox potential E^*_{ox} of our complexes were compatible with photo redox process (Table 2).[41] Additionally, semi-reversible reductive processes were observed at −1.80 V and −1.25 V vs SCE for all complexes and attributed to the reduction of the diimine ligands.[38,39,42]

Antibacterial Assays

The minimal inhibitory concentrations (MICs) of **5** to **12** were determined on four wild–type reference strains belonging to three Gram–negative species (*Pseudomonas aeruginosa* ATCC 27853, *Escherichia coli* ATCC 25922, and *Acinetobacter baumannii* CIP 70.10), and one Gram–positive cocci (*Staphylococcus aureus* ATCC 29213) (Table S3 in ESI), respectively, in the dark or upon blue (473 nm; 388 μW/cm2), green (525 nm; 238 μW/cm^2), and red light (631 nm; 320 μW/cm^2) irradiation, respectively (Figure S38 in ESI).

As shown in Figure 3, the three reference Gram–negative bacteria turned out to be significantly more resistant to the complexes than *S. aureus* under all test conditions (*i.e.*, with but also without light), suggesting a protective role of the outer membrane permeability barrier (*i.e.*, a hallmark of Gram–negatives) against these relatively hydrophobic molecules.[43] However, since differences in susceptibility were also observed between the three Gram–negative bacilli tested, other protective mechanisms were likely to be involved in the resistance to our complexes, in particular those contributing to the defense against oxidative stress.[44]

For instance, *P. aeruginosa* is considered as particularly tolerant to ROS because of the production of various pigments,[45] **5** and **6** exhibited poor antibacterial activities in the dark and in the presence of light as well, which correlates with their weak propensity to absorb visible light (see Figure 2, Table 2). The antibacterial activity of the six other complexes against the three Gram–negatives was strongly increased upon light exposure (Figure 3). Interestingly, **8** and **12** demonstrated an intrinsic activity against *E. coli* and *A. baumannii* in the dark with MICs equal to 2 or 4 mg/L, the origin of which warrants further investigations. Consistent with their photoredox properties, *i.e.*, maximum absorption wavelength and redox potential at the excited state (see above), the complexes showed maximal, intermediate, and minimal antimicrobial effects when excited with blue, green and red light, respectively. In a general manner, their antimicrobial activity correlated with their molar extinction coefficient ε. As compared with blue light irradiation, **9** and **10** drastically lost their activity when excited under green light (from 4– to 32–fold). Because of an irradiance wavelength of 525 nm, the green LEDs might irradiate at lower energy than the strong absorption bands with λ_{max} of 484–485 nm of **9** and **10** explaining the important loss of antibacterial activity (see Figure 2). Gratifyingly, **8**, **11** and **12** were able to inhibit the growth of *E. coli* (MICs equal to 2, 32 and 1 mg/L, respectively) and *A. baumannii* (4, 64 and 1 mg/L) when excited with red light, while **12** was the only compound of the series to have bacteriostatic effects against *P. aeruginosa* (2 mg/L).

Since **12** appeared as a potential candidate for PS applications, we further investigated its bactericidal activity at various concentrations and light intensities. Log phase cells of strain *P. aeruginosa* ATCC 27853 were incubated for up to 4 h in Mueller–Hinton broth supplemented with increasing concentrations of **12**, in presence of blue (388 μW/cm^2), green (238 μW/cm^2), and red (320 μW/cm^2) light, respectively.

Surviving bacteria able to form colonies (CFU) were counted after overnight subculture on drug–free Mueller–Hinton agar plates. As shown Figure 4, a concentration- and time–dependent progressive decline in viable bacteria was obtained, that

Table 2. Redox properties at ground and excited states for **5** to **12**.

Ir(IV)/Ir(III)* (V vs SCE) More reducing						
-0.75	-0.78	-0.81	-0.89	-0.92	-1.08	-2.42
$O_2/O_2^{\cdot-}$	**7**	**8**	**11** and **12**	**6**	**9** and **10**	**5**

Complex	E_{ox} (V)	E_{red} (V)	E_{00} [eV]	E^*_{ox} (V)[a]	E^*_{red} (V)[b]
$[Ir(\mathbf{L1})_2(\mathbf{L5})]^+$**5**	1.29	n.d.	3.71	−2.42	n.d.
$[Ir(\mathbf{L1})_2(\mathbf{L6})]^+$**6**	1.28	−1.46	2.16	−0.92	0.69
$[Ir(\mathbf{L2})_2(\mathbf{L5})]^+$**7**	1.20	−1.80	1.94	−0.78	0.14
$[Ir(\mathbf{L2})_2(\mathbf{L6})]^+$**8**	1.19	−1.42	1.96	−0.81	0.52
$[Ir(\mathbf{L3})_2(\mathbf{L5})]^+$**9**	1.05	−1.41	2.09	−1.08	0.67
$[Ir(\mathbf{L3})_2(\mathbf{L6})]^+$**10**	1.05	−1.25	2.09	−1.08	0.84
$[Ir(\mathbf{L4})_2(\mathbf{L5})]^+$**11**	1.11	−1.80	1.96	−0.89	0.16
$[Ir(\mathbf{L4})_2(\mathbf{L6})]^+$**12**	1.12	−1.39	1.97	−0.89	0.58

n.d. not determined. Redox potentials at excited state were approximated as follow: [a] $E^*_{red} = E_{red} - E_{00}$. [b] $E^*_{ox} = E_{ox} + E_{00}$.

Research Article
doi.org/10.1002/ejic.202300767

Chemistry Europe
European Chemical Societies Publishing

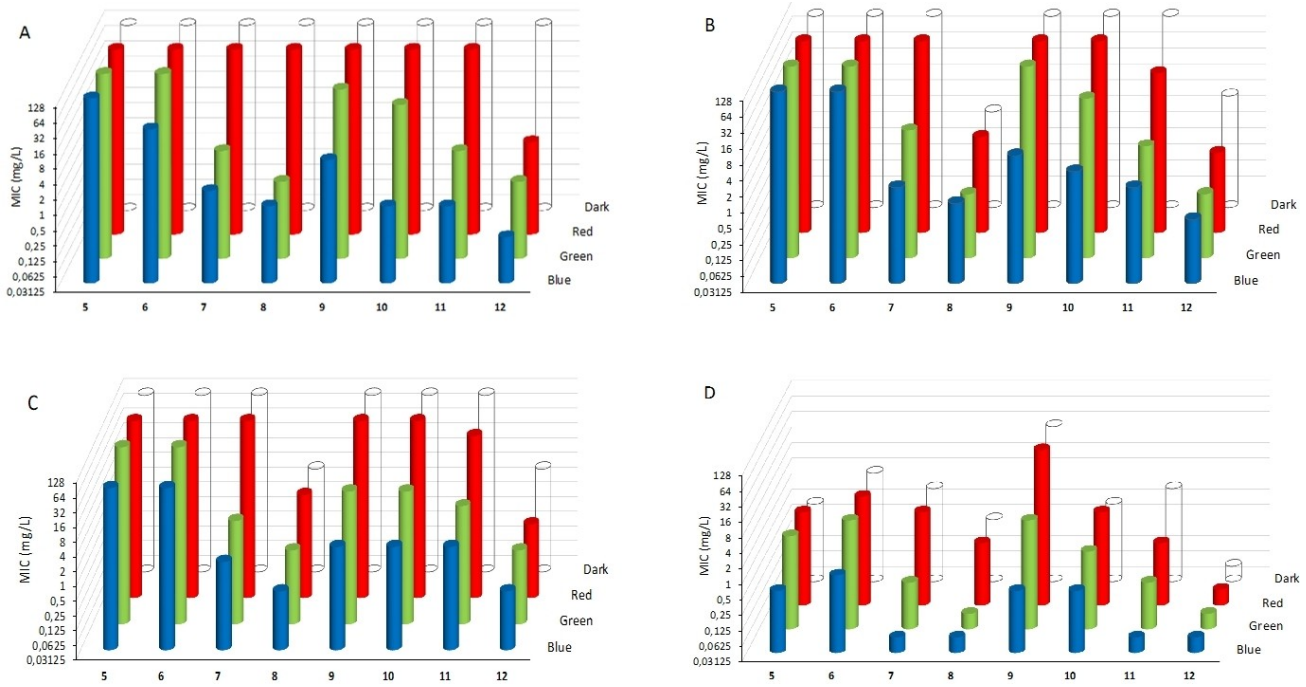

Figure 3. Susceptibility of strains (A) *P. aeruginosa* ATCC 27853, (B) *E. coli* ATCC 25922, (C) *A. baumannii* CIP 70.10, and (D) *S. aureus* ATCC 29213, to selected iridium complexes. Log phase bacteria cultivated in Mueller–Hinton broth were exposed to Log_2 increasing concentrations of complexes for 18 h ± 2, in the presence of blue light at 388 μW/cm^2, green light at 238 μW/cm^2, or red light at 320 μW/cm^2. MICs were determined and compared to those of controls grown without light exposure (dark).

was more pronounced under blue- than green- or red–light exposure, in agreement with the corresponding MIC values of the complex (0.25 mg/L, 1 mg/L, and 2 mg/L, respectively). No survivors from the initial inoculum could be detected after 2 h of exposure to 8-fold MIC of **12** activated with blue (2 mg/L), or green light (8 mg/L). The physical destruction of bacteria was confirmed by microscopic examination of the growth cultures after 18 h of incubation (Figure S39). On the other hand, illumination with red light only resulted in a delayed and partial killing at 8 mg/L, with a maximal 3 Log_{10} decrease of living bacteria after 4 h of exposure. It should be noticed that a slight bacterial regrowth was monitored at some bactericidal concentrations of **12** (4 mg/L under blue light, 8 mg/L under green light activation) (Figure 4). However, the resistance level (MIC) of these survivors to the complex was identical to that of the initial strain ATCC 27853 after subculture on drug-free agar plates (data not shown), thus ruling out possible emergence of stable resistant mutants, but rather supporting the notion of a phenotypic adaptation under certain conditions. Then, the killing effects of increasing light intensities were also investigated on strain ATCC 27853 exposed to 1 MIC of **12**, as determined previously at the lowest intensity of blue (0.25 mg/L; 388 μW/cm^2) and red LED (2 mg/; 320 μW/cm^2), respectively. As illustrated by Figures 5A and 5B, increasing light intensities both dramatically augmented the extent of bacterial killing at given time points post drug exposure, and shortened the delay at which no more survivors were detected in the bacterial cultures (i.e., $\geq$5 Log_{10} decrease in CFU from initial inoculum). For instance, a total destruction of bacteria was obtained within 1 h under blue light exposure at 1522 μW/cm^2, while 2 h of exposure were required to obtain the same result upon red light irradiation at the maximal intensity provided by the LED (1212 μW/cm^2).

No bacterial regrowth was observed in any of these experiments. Additional and concordant data are provided for various drug concentrations and LED light intensities (Figures S40 and S41). Altogether, the results reported above show that a strong and fast killing of *P. aeruginosa* can be achieved with **12**, either by increasing the compound concentration or light intensity, or both.

Photogeneration of ROS

To get some insights about the activity of our iridium complexes against bacteria, ROS detection and quantification were undertaken. As the series of iridium complexes bearing bipy ligands shown antibacterial activities on all the visible range, we focused our measurement on **6**, **8**, **10** and **12**. For that purpose, the ROS quantum yield (Φ_Δ) of **6**, **8**, **10** and **12** were experimentally determined using $[Ru(bpy)_3Cl_2]$ as benchmark ($\Phi_\Delta = 0.5746$; $E_{1/2}$ ($Ru^{III/II*}$) = −0.8147). In details, the Φ_Δ were measured using deaerated dichloromethane solutions of iridium complexes at 10^{-5} M in the presence of 1,3-diphenylisobenzofuran (DPBF) at 10^{-4} M. Of note, laser excitation was selected at 473 nm for the ROS evaluation. Indeed, the ROS quencher, *i.e.* the DPBF, was reported to self–photodegrade at 452 nm which does not allow the evaluation of ROS photo-

Research Article
doi.org/10.1002/ejic.202300767

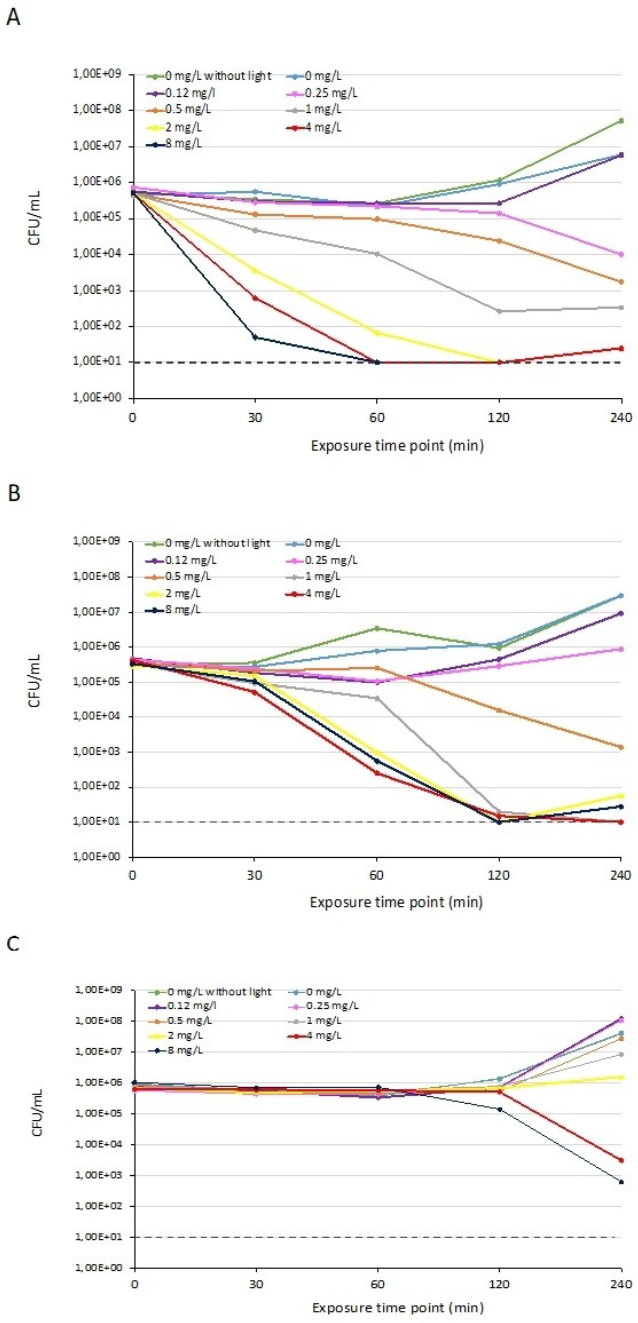

Figure 4. Concentration–dependent activity of **12** activated by (A) blue light at 388 μW/cm^2, (B) green light at 238 μW/cm^2, or red light at 320 μW/cm^2, on *P. aeruginosa* ATCC 27853. Exponentially growing cells were exposed for up to 4 h in Mueller–Hinton broth, at 35 °C, at increasing drug concentrations. Values are means of at least two independent experiments. The dotted line represents the lower limit of colony counting.

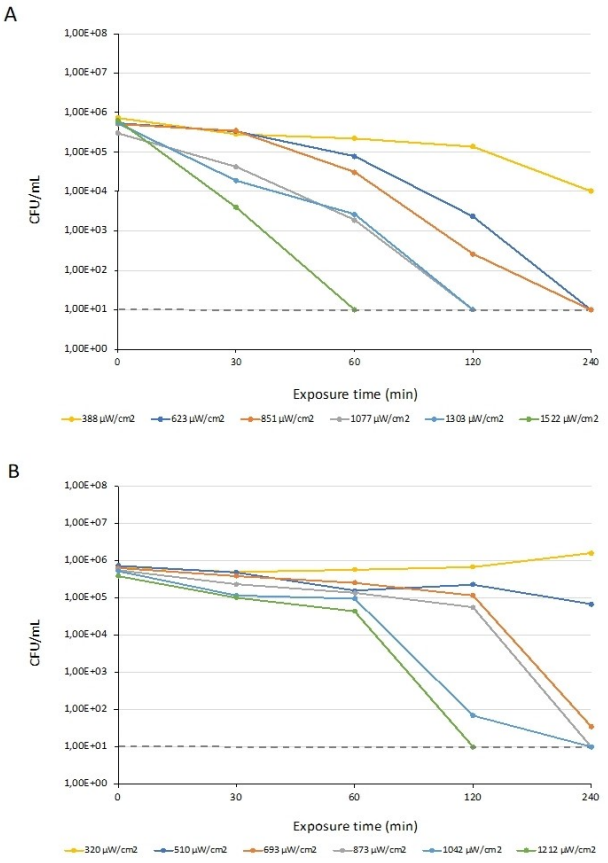

Figure 5. Light intensity–dependent activity of complex **12** activated by (A) blue or (B) red light , on *P. aeruginosa* ATCC 27853. Exponentially growing cells were exposed for up to 4 h in Mueller–Hinton broth, at 35 °C, at the MIC of complex **12** as determined at the lowest intensity of blue (MIC = 0.25 mg/L) and red light (MIC = 2 mg/L), respectively. Values are means of at least two independent experiments. The dotted line represents the lower limit of colony counting.

generation at the wavelength of the blue LED used in our susceptibility testing experiments.[48] Experimentally, the decrease in the absorption intensity of DPBF in the presence of each iridium complexes was measured and compared to the decrease in the absorption in the presence of $[Ru(bpy)_3Cl_2]$, furnishing indirectly the singlet oxygen quantum yields Φ_Δ for all our complexes (Table 3). Then, photooxidation rates of DPBF (k) were measured for **6**, **8**, **10**, **12**, and $[Ru(bpy)_3Cl_2]$ under irradiation at 473, 525 and 631 nm corresponding to blue, green and red regions, respectively. For discussion, the ε at 452, 473, 525 and 631 nm corresponding to the wavelengths of the three types of LEDs and the laser excitation used for the Φ_Δ measurement, were determined. The values of ε, Φ_Δ and k for **6**, **8**, **10**, **12**, and $[Ru(bpy)_3Cl_2]$ are reported in Table 3. As expected, complex **6** did not show any ROS production due to its weak propensity to absorb visible light. Then, **8**, **10** and **12** showed ROS generation upon blue irradiation at 473 nm in good agreement with all photophysical and electrochemical parameters, i.e. their ε at 473 nm and their compatible redox potential at excited state E_{ox}* for the generation of the oxygen radical anion. Of note, **8** and **12** exhibited a very high Φ_Δ of 73 and 94% compared to $[Ru(bpy)_3Cl_2]$ (57%), whereas **10** showed a similar Φ_Δ of 55% (Table 3).

To study the ROS generation in the green and red regions, photooxidation rates of DPBF (k) at 473, 525 and 631 nm were measured for **6**, **8**, **10**, **12**, and $[Ru(bpy)_3Cl_2]$. The values of k showed that **8**, **10** and **12** were generating ROS in blue and green regions while only **12** was oxidizing DPBF in the red zone (Figure 6). **10**, exhibiting similar Φ_Δ than $[Ru(bpy)_3Cl_2]$, had also similar values of k upon blue irradiation with 330.10^{-4} min^{-1}.

Research Article
doi.org/10.1002/ejic.202300767

Table 3. ε in function of relevant wavelengths, $^1O_2$ quantum yields (Φ_Δ) and photooxidation rates (k) for **6**, **8**, **10** and **12** and $[Ru(bpy)_3Cl_2]$ in CH_2Cl_2.

Complex	ε (10^3 $M^{-1}.cm^{-1}$)				Φ_Δ	k (10^{-4} min^{-1})		
	452 nm	473 nm	525 nm	631 nm	473 nm	473 nm	525 nm	631 nm
6	0.7				n.d.	n.d.	n.d.	n.d.
8	6.9	4.7	0.9	–	0.73	250	19	n.d.
10	63	88	2.7	–	0.55	330	13	n.d.
12	9.8	9.7	0.8	0.2	0.94	670	29	7
$[Ru(bpy)_3Cl_2]$	13	7.6	0.9	–	0.57	340	55	n.d.

n. d.: Not Detected.

8 having a lower ε of 4 700 $M^{-1}.cm^{-1}$ than $[Ru(bpy)_3Cl_2]$ (ε = 7 600 $M^{-1}.cm^{-1}$) at 473 nm but a higher Φ_Δ shown a k value of 250 10^{-4} min^{-1}. **12** possessing ε of 9.8 103 $M^{-1}.cm^{-1}$ and Φ_Δ of 94% showed the highest k of 670 10^{-4} min^{-1}. Under the green irradiation (525 nm), **8**, **10** and **12** exhibited all a lower k than $[Ru(bpy)_3Cl_2]$ even in the case of **10** possessing a high ε of 88 000 $M^{-1}.cm^{-1}$ compared to $[Ru(bpy)_3Cl_2]$ (ε = 7 600 $M^{-1}.cm^{-1}$) confirming that the green LED might irradiate with a too low energy for the excitation of **10**. Finally, **12** was found to be the sole iridium complex able to produce ROS upon red irradiation (631 nm), and a value of k at 7 10^{-4} min^{-1} was measured. In other words, only **12** was exhibiting photo–generation of ROS ability under red irradiation. This photophysical and analytical data are in good agreement with the antibacterial activities mentioned above. These encouraging preliminary data proved the compatibility of many of our PSs for antibacterial applications using light sources. Another point is that the photo-oxidation rates of DPBF k were presenting a coherent trend toward the antibacterial activity upon blue, green and red irradiation.

Activity of 12 on *P. aeruginosa* is Not Influenced by Efflux Pumps

Active efflux systems belonging to the RND (Resistance Nodulation cell Division) family of transporters are known to contribute to the natural and acquired levels of resistance of Gram–negative species to antibiotics and a variety of xenobiotics. In *P. aeruginosa*, four major RND efflux pumps tend to antagonize the activity of antibiotics more strongly than in other species, namely MexAB–OprM, MexCD–OprJ, MexEF–OprN, and MexXY/OprM.[49] These nano–machineries maintain the homeostasis of cell interior by actively rejecting a variety of structurally diverse amphiphilic molecules to the external medium. Since in our experiments *P. aeruginosa* turned out to be more resistant to iridium complexes than *E. coli* and *A. baumannii* (Figure 3), we wondered whether the Mex systems could account for such differences by impairing the intracellular accumulation of these hydrophobic molecules. However, the use of a series of mutants derived from reference strains PAO1 and PA14, lacking or overexpressing the individual pumps cited above failed to demonstrate a variation in susceptibility (MIC) to **11** and **12** in presence of blue, green, or red light (Table S4), thus providing evidence that the complexes tested are not substrates of Mex systems.

Activity of 12 on Clinical Strains of *P. aeruginosa*

Because iridium complexes were primarily developed to combat antibiotic resistant bacterial strains, we selected 14 genetically characterized clinical strains of *P. aeruginosa* exhibiting different phenotypes of resistance to antipseudomonal antibiotics, from

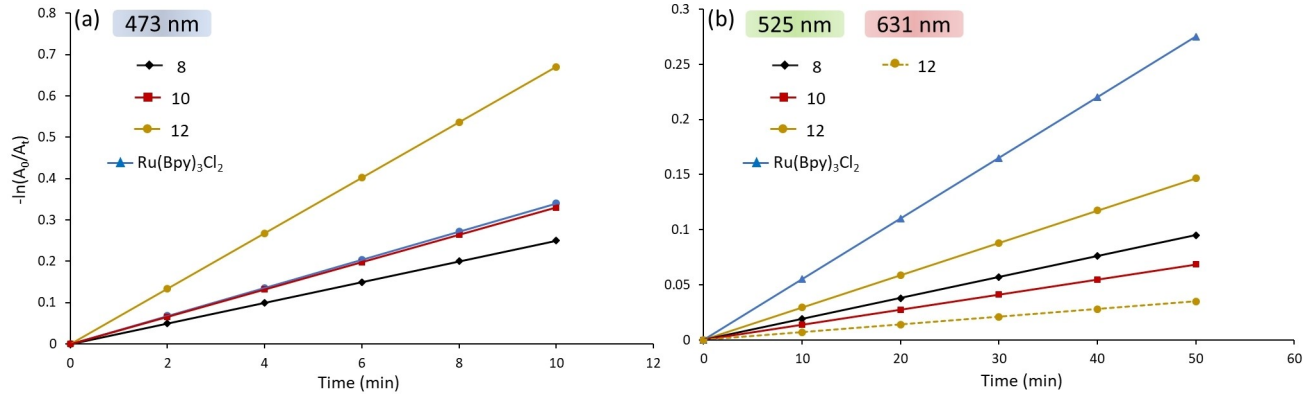

Figure 6. Kinetics of the photooxidation of DPBF in the presence of **8**, **10**, **12** and $[Ru(Bpy)_3Cl_2]$ (10^{-5} M) using laser excitation at 473 nm (a), 525 and 631 nm (b).

Research Article
doi.org/10.1002/ejic.202300767

0 (fully susceptible strains) to 12 (extensively resistant strains) molecules among the 17 tested (Table S5). Very interestingly, regardless of their resistance profiles to antibiotics, these strains exhibited the same susceptibility, within a two–fold dilution range, to **12** activated either with blue, green, or red light at 388 μW/cm^2, 238 μW/cm^2, and 320 μW/cm^2, respectively. The absence of cross–resistance between the complex and antibiotics opens the way to potential therapeutic applications against hard–to–treat strains. However, a larger panel of fully characterized multidrug resistant isolates will be necessary to ascertain that most of the many mechanisms of antibiotic resistance encountered in *P. aeruginosa* do not impact the efficacy of iridium complexes. Conversely, *in vitro* evolution experiments will be required to support the notion that treatments with these new agents will not promote the emergence of antibiotic resistant mutants or the spread of resistance plasmids.

Conclusions

This work describes the synthesis of a series of eight Ir(III) complexes (from **5** to **12**) absorbing light from UV to red regions. Irradiation with blue (452 nm), green (525 nm), or red (631 nm) LED light was found to result in impressive growth inhibitory effects on *S. aureus*. *P. aeruginosa*, *A. baumanii* and *E. coli*, especially for **7** to **12**. MIC values of some of these complexes were close to, or even lower than those reported for approved antibiotics (Table S5). This antibacterial activity was correlated with the photophysical and electrochemical properties of complexes, enabling them to generate ROS under visible light irradiation. Altogether, these findings demonstrate that the physical, chemical, and antibacterial features of such complexes may be rationalized to obtain optimized drugs. In antibacterial PDT, drugs photoactivable with red light are of outmost interest to limit damage to host tissues. **12** was the most adapted to the red–light irradiation mode. Its efficacity was remarkable on *P. aeruginosa*, a nosocomial pathogen intrinsically more resistant to antibiotics than other Gram-negative species. Very interestingly, this activity remained constant on multidrug resistant strains, including those overproducing active efflux systems and other acquired mechanisms (data not shown). The observation that the killing activity of **12** on *P. aeruginosa* can be increased at higher light intensities open interesting perspectives in the treatment of infection sites offering a limited access to drugs (*e.g.*, abscess, brain).

While all our complexes demonstrated an intrinsic activity on *S. aureus* in the absence of light, only **8** and **12** inhibited the growth of *E. coli* and *A. baumannii* at measurable concentrations, under these conditions. How the two complexes are able to partially circumvent the outer membrane permeability barrier of these two bacteria remains unclear at present. However, this suggests that the activity spectrum of organometallic PSs can be widen by increasing their ability to enter Gram-negative cells more easily. The delivery of organometallics payloads into bacteria using siderophore vectors has been recently reported.[50–52] *In vitro*, this Trojan horse strategy was able to promote the penetration of vectorized drugs into bacterial cells as compared to human cells.[50,51] The functionalization of **12** with a siderophore could be an opportunity to develop a new generation of targeted organometallic PSs photoactivable by red wavelengths, exhibiting higher antimicrobial properties and a reduced toxicity for the host.

Experimental Section

General Remarks for Synthesis

Iridium (III) chloride was bought from Alfa aesar. Coumarin C6 was purchased from Sigma Aldrich. All solvents were purchased from Carlo Erba. Deuterated solvents were purchased from Euriso–top. The ^{1}H, ^{13}C, ^{19}F and ^{31}P were recorded on a 400, 500 and 600 MHz Brücker spectrometer. Proton (^{1}H) NMR information is given in the following format: Chemical shift (δ) are reported in ppm relative to $CHCl_3$ multiplicity (s, singulet; d, doublet; t, triplet; m, multiplet), coupling constant (s) (*J*) in Hertz (Hz), number of protons. Chemical shift (δ) of carbon (^{13}C) NMR spectra are reported in ppm relative to $CDCl_3$ unless stated otherwise. HRMS analysis were performed by LCMT analytical services. Ligands and dimers were synthesized according to literature.[30,53,54]

General Procedure for the Synthesis of Iridium Complexes

In a Schlenck tube under inert atmosphere, iridium dimer (1.0 eq.) and N,N ligand (2.2 eq.) (**L 5** or **L 6**) were dissolved in 2 : 1 degassed solution of CH_2Cl_2/MeOH. The reaction mixture was stirred at 60 °C overnight. After cooling down, KPF_6 powder (10.0 eq.) was added and the mixture was stirred for 1 h at room temperature. The solution was filtered on a frit and the cake was washed using CH_2Cl_2. The mixture was concentrated under reduced pressure and solubilize in a minimum amount of CH_2Cl_2. Diethyl ether was added to afford a precipitate which was filtered on a frit and washed several times using diethyl ether and then pentane to afford pure cationic iridium complexes.

Complex **5** – Following general procedure with iridium dimer $[Ir(ppz)_2Cl]_2$ (110 mg, 0.11 mmol, 1.0 eq.) and 2,2′-dipyridylamine **L 5** (40 mg, 0.23 mmol, 2.2 eq.), complex **5** was obtained as a white solid (65 %). ^{1}H NMR (600 MHz, DMSO) δ 10.68 (s, 1 H), 8.86 (d, *J* = 2.6 Hz, 2 H), 7.87–7.75 (m, 2 H), 7.62 (d, *J* = 2.1 Hz, 2 H), 7.59–7.56 (m, 4 H), 7.39 (d, *J* = 8.2 Hz, 2 H), 6.90 (t, *J* = 7.2 Hz, 2 H), 6.83 (t, *J* = 6.6 Hz, 2 H), 6.80–6.79 (m, 2 H), 6.69 (d, *J* = 7.2 Hz, 2 H), 5.93 (d, *J* = 6.9 Hz, 2 H) ppm. Analysis was in good agreement with literature.[30]

Complex **6** – Following general procedure with iridium dimer $[Ir(ppz)_2Cl]_2$ (200 mg, 0.2 mmol, 1.0 eq.) and 2,2′-bipyridine **L 6** (67 mg, 0.44 mmol, 2.2 eq.), complex **6** was obtained as a yellow solid (67 %).^{1}H NMR (400 MHz, DMSO) δ 8.92–8.74 (m, 4 H), 8.23 (t, *J* = 7.3 Hz, 2 H), 7.98 (d, *J* = 4.9 Hz, 2 H), 7.69–7.60 (m, 4 H), 7.14 (d, *J* = 2.0 Hz, 2 H), 6.99 (t, *J* = 7.3 Hz, 2 H), 6.80 (t, *J* = 7.3 Hz, 2 H), 6.64 (t, *J* = 2.5 Hz, 2 H), 6.15 (d, *J* = 7.1 Hz, 2 H) ppm. Analysis was in good agreement with literature.[31]

Complex **7** – Following general procedure with iridium dimer $[Ir(piq)_2Cl]_2$ (135 mg, 0.11 mmol, 1.0 eq.) and 2,2′-dipyridylamine **L 5** (40 mg, 0.23 mmol, 2.2 eq.), complex **7** was obtained as an orange solid (84 %). ^{1}H NMR (500 MHz, DMSO) δ 10.98 (s, 1H), 8.96 (d, *J* = 8.5 Hz, 2H), 8.30 (d, *J* = 8.0 Hz, 2H), 8.20 (d, *J* = 6.4 Hz, 2H), 8.16 (d, *J* = 7.9 Hz, 2H), 7.92 (t, *J* = 7.3 Hz, 2H), 7.88 (t, *J* = 7.2 Hz, 2H), 7.82 (t, *J* = 8.6 Hz, 2H), 7.78 (d, *J* = 6.5 Hz, 2H), 7.48 (d, *J* = 8.4 Hz, 2H), 7.35 (d, *J* = 4.8 Hz, 2H), 7.04 (t, *J* = 7.3 Hz, 2H), 6.80 (dt, *J* = 9.3, 6.9 Hz, 4H),

Research Article
doi.org/10.1002/ejic.202300767

6.15 (d, $J=7.3$ Hz, 2H) ppm. Analysis was in good agreement with literature.[30]

Complex **8** – Following general procedure with iridium dimer $[Ir(piq)_2Cl]_2$ (400 mg, 0.4 mmol, 1.0 eq.) and 2,2′-bipyridine **L6** (137 mg, 0.88 mmol, 2.2 eq.), complex **8** was obtained as an orange solid (96%). ^{1}H NMR (400 MHz, DMSO) δ 9.00 (d, $J=5.2$ Hz, 2H), 8.91 (d, $J=7.9$ Hz, 2H), 8.37 (d, $J=7.9$ Hz, 2H), 8.26 (t, $J=7.6$ Hz, 2H), 8.13–8.05 (m, 2H), 7.94–7.86 (m, 4H), 7.73 (d, $J=4.8$ Hz, 2H), 7.67 (d, $J=6.5$ Hz, 2H), 7.65 (d, $J=6.2$ Hz, 2H), 7.61 (d, $J=6.3$ Hz, 2H), 7.51 (d, $J=6.4$ Hz, 2H), 7.13 (t, $J=7.4$ Hz, 2H), 6.91 (t, $J=7.3$ Hz, 2H), 6.20 (d, $J=7.5$ Hz, 2H) ppm. Analysis was in good agreement with literature.[31]

Complex **9** – Following general procedure with iridium dimer $[Ir(C_6C)_2Cl]_2$ (50 mg, 0,0265 mmol, 1.0 eq.) and 2,2′-dipyridylamine **L5** (10 mg, 0.058 mmol, 2.2 eq.), complex **9** was obtained as an orange solid (61%). ^{1}H NMR (600 MHz, $CDCl_3$) δ 9.78 (s, 2H), 7.91 (d, $J=6.4$ Hz, 2H), 7.77–7.66 (m, 6H), 7.37 (s, 2H), 7.26 (s, 2H), 7.14 (s, 2H), 6.72 (s, 2H), 6.44 (d, $J=7.2$ Hz, 2H), 6.32 (s, 1H), 6.09 (d, $J=8.4$ Hz, 1H), 5.87 (d, $J=7.3$ Hz, 2H), 3.29 (d, $J=4.9$ Hz, 8H), 1.10 (s, 12H) ppm. ^{13}C NMR (151 MHz, $CDCl_3$) δ 178.9 (2 C), 157.7 (2 C), 155.1 (2 C), 152.6 (2 C), 151.4 (2 C), 150.5 (2 C), 149.0 (2 C), 140.8 (2 C), 131.8 (2 C), 131.2 (2 C), 128.1 (2 C), 125.3 (2 C), 123.4 (2 C), 122.3 (2 C), 119.8 (2 C), 117.8 (2 C), 117.3 (2 C), 117.2 (2 C), 109.6 (2 C), 97.0 (2 C), 44.8 (4 C), 12.6 (4 C) ppm. ^{31}P NMR (243 MHz, $CDCl_3$) δ −144.3 (hept, $J=714.1$ Hz) ppm. ^{19}F NMR (565 MHz, $CDCl_3$) δ −73.0 (d, $J=714.1$ Hz) ppm. HR-MS (ACN m/z): calculated for $C_{50}H_{43}N_7O_4S_2{}^{193}Ir$ ($[M–PF_6]^+$), 1062.2447; found 1062.2461.

Complex **10** – Following general procedure with iridium dimer $[Ir(C_6C)_2Cl]_2$ (75 mg, 0.0407 mmol, 1.0 eq.) and 2,2′-bipyridine **L6** (14 mg, 0.087 mmol, 2.2 eq.), complex **10** was obtained as an orange solid (49%). ^{1}H NMR (600 MHz, $CDCl_3$) δ 8.57 (d, $J=8.0$ Hz, 2H), 8.52 (d, $J=4.9$ Hz, 2H), 8.24 (td, $J=8.0$, 1.3 Hz, 2H), 7.81 (d, $J=7.9$ Hz, 2H), 7.68–7.61 (m, 2H), 7.24 (d, $J=7.6$ Hz, 2H), 6.97–6.91 (m, 2H), 6.37 (d, $J=2.2$ Hz, 2H), 6.03 (d, $J=9.4$ Hz, 2H), 5.86 (dd, $J=9.5$, 2.6 Hz, 2H), 5.79 (d, $J=8.5$ Hz, 2H), 3.34–3.23 (m, 8H), 1.09 (t, $J=7.1$ Hz, 12H) ppm. ^{13}C NMR (151 MHz, $CDCl_3$) δ 180.6 (2 C), 177.9 (2 C), 158.1 (2 C), 156.2 (2 C), 155.2 (2 C), 152.8 (2 C), 149.8 (2 C), 147.9 (2 C), 142.1 (2 C), 132.2 (2 C), 131.3 (2 C), 129.0 (2 C), 128.2 (2 C), 125.9 (2 C), 125.3 (2 C), 123.5 (2 C), 121.8 (2 C), 118.8 (2 C), 115.8 (2 C), 109.9 (2 C), 96.9 (2 C), 44.9 (4 C), 12.6 (4 C) ppm. ^{31}P NMR (243 MHz, $CDCl_3$) δ −144.0 (hept, $J=712.7$ Hz) ppm. ^{19}F NMR (565 MHz, $CDCl_3$) δ −71.7 (d, $J=712.7$ Hz) ppm. HRMS (ACN m/z): calculated for $C_{50}H_{42}N_6O_4S_2{}^{193}Ir$ ($[M–PF_6]^+$), 1047.2338; found 1047.2356.

Complex **11** – Following general procedure with iridium dimer $[Ir(tiq)_2Cl]_2$ (200 mg, 0.16 mmol, 1.0 eq.) and 2,2′-dipyridylamine **L5** (65 mg, 0.38 mmol, 2.2 eq.), complex **11** was obtained as a brown solid (48%). ^{1}H NMR (600 MHz, $CDCl_3$) δ 10.10 (s, 1H), 8.85–8.79 (m, 2H), 7.96 (d, $J=6.4$ Hz, 2H), 7.91–7.87 (m, 4H), 7.77–7.73 (m, 4H), 7.63 (ddd, $J=8.7$, 7.2, 1.7 Hz, 2H), 7.44 (dd, $J=6.0$, 1.7 Hz, 2H), 7.41 (d, $J=4.9$ Hz, 2H), 7.32 (d, $J=6.4$ Hz, 2H), 6.65–6.60 (m, 2H), 6.15 (d, $J=4.9$ Hz, 2H) ppm. ^{13}C NMR (151 MHz, $CDCl_3$) δ 165.1 (2 C), 158.0 (2 C), 151.7 (2 C), 150.0 (2 C), 142.1 (2 C), 139.5 (2 C), 137.0 (2 C), 135.8 (2 C), 132.7 (2 C), 132.1 (2 C), 130.1 (2 C), 128.6 (2 C), 127.6 (2 C), 126.9 (2 C), 124.5 (2 C), 119.3 (2 C), 119.0 (2 C), 117.0 (2 C) ppm. ^{31}P NMR (243 MHz, $CDCl_3$) δ −143.9 (hept, $J=713.7$ Hz) ppm. ^{19}F NMR (565 MHz, $CDCl_3$) δ −71.7 (d, $J=713.7$ Hz) ppm. HRMS (ACN m/z): calculated for $C_{36}H_{25}N_5S_2{}^{193}Ir$ ($[M–PF_6]^+$), 784.1181; found 784.1185.

Complex **12** – Following general procedure with iridium dimer $[Ir(tiq)_2Cl]_2$ (150 mg, 0,12 mmol, 1.0 eq.) and 2,2′-bipyridine **L6** (40 mg, 0,26 mmol, 2.2 eq.), complex **12** was obtained as a brown solid (76%). ^{1}H NMR (600 MHz, $CDCl_3$) δ 8.84 (d, $J=8.4$ Hz, 2H), 8.72 (d, $J=8.2$ Hz, 2H), 8.15 (td, $J=8.0$, 1.5 Hz, 2H), 7.88–7.81 (m, 4H), 7.78–7.71 (m, 4H), 7.53 (d, $J=4.9$ Hz, 2H), 7.44 (ddd, $J=7.5$, 5.5, 0.9 Hz, 2H), 7.32 (d, $J=6.5$ Hz, 2H), 7.22 (d, $J=6.5$ Hz, 2H), 6.34 (d, $J=4.9$ Hz, 2H) ppm. ^{13}C NMR (151 MHz, $CDCl_3$) δ 164.9 (2 C), 158.3 (2 C), 155.9 (2 C), 150.8 (2 C), 141.2 (2 C), 140.1 (2 C), 136.9 (2 C), 136.0 (2 C), 133.1 (2 C), 132.2 (2 C), 130.4 (2 C), 128.8 (2 C), 128.4 (2 C), 127.6 (2 C), 126.9 (2 C), 125.6 (2 C), 124.4 (2 C), 119.7 (2 C) ppm. ^{31}P NMR (243 MHz, $CDCl_3$) δ −144.3 (hept, $J=712.8$ Hz) ppm. ^{19}F NMR (565 MHz, $CDCl_3$) δ −73.1 (d, $J=712.8$ Hz) ppm. HRMS (ACN m/z): calculated for $C_{36}H_{24}N_4S_2{}^{193}Ir$ ($[M–PF_6]^+$), 769.1051; found 769.1072.

Photophysical Experiments

UV-visible absorption spectra were measured at room temperature in CH_2Cl_2 (10^{-5} mol.L^{-1}) on a Perkin Elmer Lambda 40 UV-visible spectrometer; wavelengths are given in nm and extinction coefficients ε are presented in L.mol^{-1}cm^{-1}. Emission spectra were recorded in dichloromethane solution (10^{-6} mol.L^{-1}) on an Edinburgh Instrument FS5 Spectrofluorometer. The excited state lifetimes were recorded at room temperature in the solid state on a Horiba Scientific DeltaFlex TCSPC Spectrometer.

Chemical Quantum Yields Determination Φ_Δ

To determine the singlet oxygen species chemical quantum yield Φ_Δ, a comparative spectrometric method was carried out and the following equation was used:

$$\Phi_\Delta = \frac{k I_{abs/s}}{k_s I_{abs}} \Phi_{\Delta s}$$

Φ_Δ is the chemical quantum yield, $\Phi_{\Delta s}$ is the chemical quantum yield of $[Ru(bpy)_3][Cl]_2$, used as reference with $\Phi_{\Delta s}=0.57$, k is the slope obtain during the study of the decrease of the absorption of DPBF (1,3-diphenylisobenzofuran) at 410 nm when the studied complex was added. ks is the slope obtain for the study of the decrease of the absorption of DPBF at 410 nm when $[Ru(bpy)_3][Cl]_2$ was added. Iabs/s corresponds to the absolute intensity value of absorption of $[Ru(bpy)_3][Cl]_2$ at 473 nm at a concentration of 10^{-5} M. Iabs corresponds to the absolute value of absorption of the studied iridium complex at 473 nm for a concentration of 10^{-4} M. Absorbance of our oxygen singlet scavenger should be outside the absorbance maxima of our complexes and should not absorb light in the blue region. 1,3-Diphenylisobenzofuran, DPBF, was choose because of its absorption maxima at 410 nm and its lack of absorption at the chosen photoexcitation wavelength (473 nm). With photoexcitation at 473 nm, no auto photodegradation of DPBF was observed. To obtain the slope k of the reference photosensitizer, $[Ru(bpy)_3][Cl]_2$, a mixture of 10^{-5} M $[Ru(bpy)_3][Cl]_2$ and 10^{-4} M of DPBF in acetonitrile was prepared. The solution was loaded in a 1 cm quartz cuvette and a first UV-Visible spectra was recorded at t_0. It was then carried in a dark glass container, to avoid auto–photodegradation of DPBF with natural light. The mixture was then aerated three times using a Pasteur pipette and then irradiated at 473 nm for 2 min using the lamp of an Edinburgh Instrument FS5 Spectrofluorometer with emission and excitation bandwidth set at 2.0. The cuvette was then carried back to the UV-Visible spectrometer in dark glass container and the UV-Visible spectra was recorded. This process was carried out several time until t = 10 min of irradiation. A consumption of DPBF was observed and is reported in Table S1.

Cyclic Voltammetry

Cyclic voltammetry experiments were carried out on an Autolab PGSTAT101 potentiostat unit from Metrohm with the Nova software package. A glassy carbon working electrode, a platinum wire auxiliary electrode and an Ag/AgCl (3 M KCl) as reference electrode were used in a standard three-electrode configuration. Cyclic voltammetry was performed in a 0.1 M anhydrous degassed solution of $n\mathrm{Bu_4NPF_6}$ in acetonitrile at a scanning rate of 0.1 $\mathrm{V.s^{-1}}$. Values were calibrated using ferrocene as reference.

Bacterial Strains and Growth Conditions

The bacterial strains used in this study are listed in Table S5. Depending on the experiments, bacteria were cultivated either overnight on Mueller–Hinton agar plates (MHA, Fisher Scientific, Illkirch, France) or in Mueller–Hinton broth (MHB) containing from 20 to 25 μg/mL Ca^{2+} and from 10 to 12.5 μg/mL Mg^{2+} (Becton Dickinson and Company, Cockeysville, MD, USA). All cultures were performed aerobically at 35 °C. Stock solutions of iridium complexes were prepared in dimethyl sulfoxide (DMSO) at 10.2 mg/mL final concentration, and stored in the dark at −20 °C until use.

Antimicrobial Susceptibility Testing

Minimum inhibitory concentrations (MIC) of iridium complexes were determined by the serial twofold macrodilution method recommended by the CLSI (Clinical and Laboratory Standards Institute, 2006).[55] Test cultures were performed in 1.5 mL translucid microtubes (Dutscher, Bernoslheim, France), each containing 100 μL of MHB inoculated with 2.5 10^5 CFU/mL log phase bacteria and individual photosensitizers at a final concentration ranging from 0.06 to 128 μg/mL (*i.e.*, which corresponds to the solubility limit of these hydrophobic compounds). The final concentration of DMSO did not exceed 5% of the culture volume. As illustrated Figure S18, the microtubes were incubated at 35 °C in a water–bath, and were transilluminated with a blue, green, or red light emitted by a laterally positioned LED, for the desired time length. Controls were carried out in parallel under the same conditions, though in the dark. The bactericidal activity of complex **12** was assessed on Pseudomonas aeruginosa wild–type reference strain ATCC 27853, at final concentrations ranging from 0.5 to 16 μg/mL and under the same conditions as those described above for MIC experiments. Illuminated samples were run in parallel to controls grown in the dark. At time 0 min, 30 min, 1 h, 2 h and 4 h of incubation, colony–forming (surviving) bacteria were counted after overnight culture on drug-free MHA plates inoculated with an automatic Spiral Plater automat (easySpiral Pro®, Interscience, Saint–Nom–la–Bretèche, France). Both MIC and killing experiments were at least repeated twice to ascertain results.

Supporting Information

The authors have cited additional references within the Supporting Information.[56,57]

Author Contributions

G. L. A. M, P. P., S. G. and J. L. R. wrote the manuscript with inputs from the others authors. G. L. A. M. supervised organic chemistry experiments. S. G. and J. L. R. supervised organometallic chemistry and photophysical studies. P. P. supervise microbiology experiments. A. L. F. contributes to organic synthesis. J. R. synthesized, purified and characterized iridium compounds **1** to **12**. J. R. did the photophysical and electrochemical characterization as well as the ROS generation study. J. C. and P. P. evaluated the antibacterial activities of iridium complexes. G. L. A. M., S. G. and P. P. found the grants.

Acknowledgements

All authors acknowledge the Agence Nationale pour la Recherche (VECTRIUM project, ANR 19-CE18-0011-02) for financial support and for PhD fellowships attributed to ALF and JR. GLAM warmly thanks Vaincre la Mucoviscidose and the Association Grégory Lemarchal (French associations against cystic fibrosis) for repeated financial support. GLAM also acknowledges the Interdisciplinary Thematic Institute (ITI) InnoVec (Innovative Vectorization of Biomolecules, IdEx, ANR-10-IDEX-0002), the SFRI (ANR-20-SFRI-0012) and CNRS for financial support. Authors also acknowledge the Centre National de la Recherche Scientifique (CNRS) and the "Ministère de la Recherche et des Nouvelles Technologies" for general financial support. S. G. acknowledges the LABEX SynOrg (ANR-11-LABX-0029) for financial support. We are grateful to the French National Reference Center for antibiotic resistance (Maxime Bour, Pauline Triponney) for supplying multidrug resistant strains of *P. aeruginosa*.

Conflict of Interests

The authors declare no conflict of interest.

Data Availability Statement

The data that support the findings of this study are available in the supplementary material of this article.

Keywords: Iridium (III) Complexes · Photodynamic therapy · Photosensitizer · ROS · *Pseudomonas aeruginosa*

[1] N. K. Prasad, I. B. Seiple, R. T. Cirz, O. S. Rosenberg, *Antimicrob. Ag. Chemother.* **2022**, *66*, e0005422.
[2] L. J. V. Piddock, *Lancet* **2016**, *16*, 767.
[3] R. L. Lucaciu, A. C. Hangan, B. Sevastre, L. S. Oprean, *Molecules* **2022**, *27*, 6485.
[4] P. V. Simpson, N. M. Desai, I. Casari, M. Massi, M. Falasca, *Future Med. Chem.* **2019**, *11*, 119.
[5] I. Ott, R. Gust, *Arch. Pharm.* **2007**, *340*, 117.
[6] M. Yamashita, *Int. Immunopharmacol.* **2021**, *101*, 108272.
[7] L. M. Lim, N. Ly, D. Anderson, J. C. Yang, L. Macander, A. Jarkowski III, A. Forrest, J. B. Bulitta, B. T. Tsuji, *Pharmacotherapy* **2010**, *30*, 1279.
[8] A. Frei, J. Zuegg, A. G. Elliott, M. Baker, S. Braese, C. Brown, F. Chen, C. G. Dowson, G. Dujardin, N. Jung, A. P. King, A. M. Mansour, M. Massi, J. Moat, H. A. Mohamed, A. K. Renfrew, P. J. Rutledge, P. J. Sadler, M. H. Todd, C. E. Willans, J. J. Wilson, M. A. Cooper, M. A. T. Blaskovich, *Chem. Sci.* **2020**, *11*, 2627.
[9] A. Frei, *Antibiotics* **2020**, *9*, 90.

[10] M. Patra, G. Gasser, N. Metzler-Nolte, *Dalton Trans.* **2012**, *41*, 6350.
[11] R. Youf, R. Ghanem, A. Nasir, G. Lemercier, T. Montier, T. Le Gall, *Biofilm* **2023**, *5*, 100113.
[12] R. Youf, A. Nasir, M. Müller, F. Thétiot, T. Haute, R. Ghanem, U. Jonas, H. Schönherr, G. Lemercier, T. Montier, T. Le Gall, *Pharmaceutica* **2022**, *14*, 1664.
[13] A. Jain, N. T. Garrett, Z. P. Malone, *Photochem. Photobiol.* **2022**, *98*, 6.
[14] F. Heinemann, J. Karges, G. Gasser, *Acc. Chem. Res.* **2017**, *50*, 2727.
[15] B. F. Hohlfeld, B. Gitter, C. J. Kingsbury, K. J. Flanagan, D. Steen, G. D. Wieland, N. Kulak, M. O. Senge, A. Wiehe, *Chem. Eur. J.* **2021**, *27*, 6440.
[16] B. Liu, S. Monro, M. A. Jabed, C. G. Cameron, K. L. Colón, W. Xu, S. Kilina, S. A. McFarland, W. Sun, *Photochem. Photobiol. Sci.* **2019**, *18*, 2381.
[17] L. Wang, S. Monro, P. Cui, H. Yin, B. Liu, C. G. Cameron, W. Xu, M. Hetu, A. Fuller, S. Kilina, S. A. McFarland, W. Sun, *ACS Appl. Mater. Interfaces* **2019**, *11*, 3629.
[18] E. Sauvageot, M. Elie, S. Gaillard, R. Daniellou, P. Fechter, I. J. Schalk, V. Gasser, J.-L. Renaud, G. L. A. Mislin, *Metallomics* **2017**, *9*, 1820.
[19] S.-Y. Takizawa, R. Aboshi, S. Murata, *Photochem. Photobiol. Sci.* **2011**, *10*, 895.
[20] L. Zhou, F. Wei, J. Xiang, H. Li, C. Li, P. Zhang, C. Liu, P. Gong, C. Cai, K. M.-C. Wong, *Chem. Sci.* **2020**, *11*, 12212.
[21] C. Caporale, M. Massi, *Coord. Chem. Rev.* **2018**, *363*, 71.
[22] R. Yin, T. Dai, P. Avci, A. E. Jorge, W. C. de Melo, D. Vecchio, Y. Y. Huang, A. Gupta, M. R. Hamblin, *Curr. Opin. Pharmacol.* **2013**, *13*, 731.
[23] P. E. Hockberger, T. A. Skimina, V. E. Centonze, C. Lavin, S. Chu, S. Dadras, J. K. Reddy, J. G. White, *Proc. Nat. Acad. Sci.* USA, **1999**, *96*, 6255.
[24] M. Wegener, M. J. Hansen, A. J. M. Driessen, W. Szymanski, B. L. Feringa, *J. Am. Chem. Soc.* **2017**, *139*, 17979.
[25] R. Weissleder, *Nat. Biotechnol.* **2001**, *19*, 316.
[26] H. Huang, S. Banerjee, P. J. Sadler, *ChemBioChem.* **2018**, *19*, 1574.
[27] A. Tsuboyama, H. Iwawaki, M. Furugori, T. Mukaide, J. Kamatani, S. Igawa, T. Moriyama, S. Miura, T. Takiguchi, S. Okada, M. Hoshino, K. Ueno, *J. Am. Chem. Soc.* **2003**, *125*, 12971.
[28] M. Nonoyama, *Bull. Chem. Soc. Jpn.* **1974**, *47*, 767.
[29] M. Nonoyama, *J. Org. Chem.* **1975**, *86*, 263.
[30] E. Sauvageot, R. Marion, F. Sguerra, A. Grimault, R. Daniellou, M. Hamel, S. Gaillard, J.-L. Renaud, *Org. Chem. Front.* **2014**, *1*, 639.
[31] E. Sauvageot, P. Lafite, E. Duverger, R. Marion, M. Hamel, S. Gaillard, J.-L. Renaud, R. Daniellou, J. Organomet, *Chem.* **2016**, *808*, 122.
[32] S. Takizawa, C. Pérez-Bolívar, P. Anzenbacher, S. Murata, *Eur. J. Inorg. Chem.* **2012**, *2012*, 3975.
[33] L. M. Groves, C. Schotten, J. Beames, J. A. Platts, S. J. Coles, P. N. Horton, D. L. Browne, S. J. Pope, *Chem. Eur. J.* **2017**, *23*, 9407.
[34] A. Kapturkiewicz, A. Kamecka, *A. RSC Adv.* **2021**, *11*, 29308.
[35] S.-J. Liu, Q. Zhao, Q.-L. Fan, W. Huang, *Eur. J. Inorg. Chem.* **2008**, *2008*, 2177.
[36] C. Huang, C. Liang, T. Sadhukhan, S. Banerjee, Z. Fan, T. Li, Z. Zhu, P. Zhang, K. Raghavachari, H. Huang, *Angew. Chem. Int. Ed.* **2021**, *60*, 9474.
[37] A. Tsuboyama, H. Iwawaki, M. Fugugori, T. Mukaide, J. Kamatani, S. Igawa, T. Moriyama, S. Miura, T. Takiguchi, S. Okada, M. Hoshino, K. Ueno, *J. Am. Chem. Soc.* **2003**, *125*, 12971.
[38] J. D. Slinker, A. A. Gorodetsky, M. S. Lowry, J. Wang, S. Parker, R. Rohl, S. Bernhard, G. Malliaras, *J. Am. Chem. Soc.* **2004**, *126*, 2763.
[39] S. Lowry, J. I. Goldsmith, J. D. Slinker, R. Rohl, R. A. Jr Pascal, G. Malliaras, S. Bernhard, *Chem. Mater.* **2005**, *17*, 5712.
[40] R. Bevernaegie, S. A. M. Wehlin, B. Elias, L. A. Troian-Gautier, *ChemPhotoChem.* **2021**, *5*, 217.
[41] A. A. Abdel-Shafi, P. D. Beer, R. J. Mortimer, F. Wilkinson, J. Phys, *Chem. A.* **2000**, *104*, 192.
[42] L. Zang, H. Zhao, X. Ji, W. Cao, Z. Zhang, P. Meng, *Photochem. Photobiol. Sci.* **2017**, *16*, 1088.
[43] H. Nikaido, *Microbiol. Mol. Biol. Rev.* **2003**, *67*, 593.
[44] W. S. Cruz Nizer, V. Inkovskiy, Z. Versey, N. Strempel, E. Cassol, J. Overhage, *Pathogenesis* **2021**, *10*, 1187.
[45] V. T. Orlandi, F. Bolognese, L. Chiodaroli, T. Tolker-Nielsen, P. Barbieri, *Microbiology* **2015**, *161*, 2298.
[46] K. Krumova, G. Cosa, S. Nonell, C. Flors, *The Royal Society of Chemistry* **2016**, *1*, 1.
[47] C. K. Prier, D. A. Rankic, D. W. C. MacMillan, *Chem. Rev.* **2013**, *113*, 5322.
[48] K. K.-W. Lo, C.-K. Li, J. S.-Y. Lau, *Organometallics* **2005**, *24*, 4594.
[49] X. Z. Li, P. Plésiat, H. Nikaido, *Clin. Microb. Rev.* **2015**, *28*, 337.
[50] Q. Laurent, L. K. Batchelor, P. J. Dyson, *Organometallics* **2018**, *37*, 915.
[51] C. Guo, E. M. Nolan, *J. Am. Chem. Soc.* **2022**, *144*, 12756.
[52] J. Southwell, R. Herman, D. Raines, J. Clarke, I. Boeswald, T. Dreher, S. Gutenthaler, N. Schubert, J. Seefeldt, N. Metzler-Nolte, G. Thomas, K. Wilson, A.-K. Duhme-Klair, *Chem. Eur. J.* **2023**, *29*, e202202536.
[53] S. Lamansky, P. Djurovich, D. Murphy, F. Abdel-Razzaq, H.-E. Lee, C. Adachi, P. E. Burrows, S. R. Forrest, M. E. Thompson, *J. Am. Chem. Soc.* **2001**, *123*, 4304.
[54] C. Yang, F. Mehmood, T. L. Lam, S. L.-F. Chan, Y. Wu, C.-S. Yeung, X. Guan, K. Li, C. Y.-S. Chung, C.-Y. Zhou, T. Zou, C.-M. Che, *Chem. Sci.* **2016**, *7*, 3123.
[55] Clinical and Laboratory Standards Institute **2006**. Methods for dilution antimicrobial susceptibility tests for bacteria that grow aerobically; approved standard–seven edition (document M7–A7, Vol. 26, No 2), Wayne, PA, USA.
[56] L. G. Rahme, E. J. Stevens, S. F. Wolfort, J. Shao, R. G. Tompkins, F. M. Ausubel, *Science* **1995**, *268*, 1899.
[57] A. Tetard, A. Zedet, C. Girard, P. Plésiat, C. Llanes, *Antimicrob. Agents Chemother.* **2019**, *63*, e1081–e1019.

Manuscript received: December 18, 2023
Revised manuscript received: March 21, 2024
Accepted manuscript online: April 2, 2024
Version of record online: ■■, ■■

RESEARCH ARTICLE

A new iridium complex, based on a combination of 2-thiophenyl-isoquinoline as cyclometallating ligand and bipyridine was synthesized. This complex was applied as photosensitizer both for the photogeneration of reactive oxygen species leading to antibacterial activities upon red LED (Light Emitting Diode) irradiation and demonstrating very interesting potential for Photodynamic Therapy against highly resistant Gram– negative bacteria.

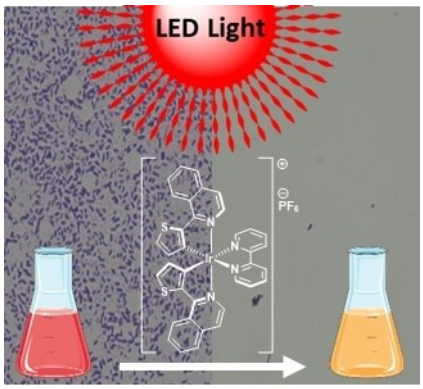

Dr. J. Renault, J. Couchot, Dr. A. L. Faucon, Prof. J.-L. Renaud, Dr. G. L. A. Mislin, Prof. P. Plésiat*, Dr. S. Gaillard**